Positron lymphography via intracervical ^{18}F-FDG injection for pre-surgical lymphatic mapping in cervical and endometrial malignancies

Jennifer J Mueller,[1,2] Lawrence T. Dauer,[3] Rajmohan Murali,[4] Alexia Iasonos,[5] Neeta Pandit-Taskar,[6] Nadeem R. Abu-Rustum,[1,2] Jan Grimm[6,7,8,9]

[1]Gynecology Service, Department of Surgery, Memorial Sloan Kettering Cancer Center, New York, NY
[2]Department of Obstetrics and Gynecology, Weill Cornell Medical College, New York, NY
[3]Department of Radiology, Memorial Sloan Kettering Cancer Center, New York, NY
[4]Department of Pathology, Memorial Sloan Kettering Cancer Center, New York, NY
[5]Department of Epidemiology and Biostatistics, Memorial Sloan Kettering Cancer Center, New York, NY
[6]Molecular Pharmacology Program, Memorial Sloan Kettering Cancer Center, New York, NY
[7]Department of Radiology, Memorial Sloan Kettering Cancer Center, New York, NY
[8]Pharmacology Program, Weill Cornell Medical College, New York, NY
[9]Department of Radiology, Weill Cornell Medicine, New York, NY

Corresponding author:
Jan Grimm, MD, PhD
Department of Radiology
Memorial Sloan Kettering Cancer Center
1275 York Avenue
New York, NY 10065
Tel. 646-888-3095
grimmj@mskcc.org
ORCID-ID: 0000-0002-5282-9385

First author:
Jennifer J. Mueller, MD
Gynecology Service, Department of Surgery
Memorial Sloan Kettering Cancer Center
1275 York Avenue
New York, NY 10065
Tel. 212-639-8229
muellerj@mskcc.org

Word count: 4359

Clinical positron lymphography

Abstract

Rationale: The presence of metastasis in local lymph nodes (LNs) is a key factor influencing choice of therapy and prognosis in cervical and endometrial cancers; therefore, the exploration of sentinel LNs (SLNs) is highly important. Currently, however, SLN mapping requires LN biopsy for pathologic evaluation, since there are no clinical imaging approaches that can identify tumor-positive LNs in early stages. Staging lymphadenectomy poses risks, such as leg lymphedema or lymphocyst formation. Furthermore, in 80% to 90% of patients, the explored LNs are ultimately tumor free, meaning the vast majority of patients are unnecessarily subjected to lymphadenectomy.

Methods: Current lymphoscintigraphy methods only identify the anatomic location of the SLNs but do not provide information on their tumor status. There are no non-invasive methods to reliably identify metastases in LNs before surgery. We have developed positron lymphography (PLG), a method to detect tumor-positive LNs, where ^{18}F-fluoro-2-deoxy-D-glucose (^{18}F-FDG) is injected interstitially into the uterine cervix the day of surgery, and its rapid transport through the lymphatic vessels to the SLN is then visualized with dynamic positron emission tomography/computed tomography (PET/CT). We previously showed that PLG was able to identify metastatic LNs in animal models. Here, we present the first results from our pilot clinical trial (clinical trials identifier NCT02285192) in 23 patients with uterine or cervical cancer. On the morning of surgery, ^{18}F-FDG was injected into the cervix, followed by an immediate dynamic PET/CT scan of the pelvis and a delayed 1-h whole body scan.

Results: There were 3 (15%) node-positive cases on final pathologic analysis, and all of these LNs (including one with a focus of only 80 tumor cells) were identified by PLG. There were 2 (10%) false-positive cases with PLG, in which final pathology of the corresponding SLNs was negative for tumor.

Conclusions: This first-in-human study of PLG in women with uterine and cervical cancer demonstrates its feasibility and its ability to identify patients with nodal metastases, and warrants further evaluation in additional studies.

Introduction

Sentinel lymph node (SLN) mapping plays a central role in the detection of clinically relevant lymph nodes (LNs), replacing more invasive, less targeted approaches to nodal staging. The identification of the 'sentinel' node or nodes—the primary draining LN(s) in a given malignancy—is now an established approach in the staging of tumors across a range of disease sites, and the technique has been adopted using various dyes, radiotracers, and imaging modalities. The concept of the SLN was first described in parotid gland cancer by Gould et al in 1960 (*1*), and later explored more broadly in penile cancer by Cabanas et al in the 1970s (*2*). SLN mapping and biopsy are now cornerstones of care and are performed routinely for apparent early-stage endometrial and cervical cancers (*3-9*).

Establishing nodal status is an important factor in patient management. The detection of a pathologically positive LN influences not only stage and prognosis in many cancers but also informs decisions on adjuvant treatment. Comprehensive LN dissection is not without attendant morbidity, however, and a significant number of patients who undergo lymphadenectomy experience disfiguring and painful leg lymphedema (*10*). These patients also incur intraoperative risk, including vascular and nerve injury and prolongation of operative time (*10-12*), as well as other concerns that can include larger skin incisions, lymphocele formation, and impaired wound healing and risk of infection. SLN assessment is associated with much lower morbidity than comprehensive lymphadenectomy and is now an integral procedure in the staging and prognostication of many cancers, e.g., the vast majority of endometrial and cervical malignancies (*3, 6, 13-16*), breast cancer (*17*), and melanoma (*18*).

Although nodal evaluation is important for prognostic assessment, risk stratification and adjuvant treatment decisions, only few SLNs are found to be positive for cancer. In a study of 266 patients with endometrial cancer at our institution, only 12% of SLNs were positive on final

pathology (*6*). In a study of 2,001 patients with melanoma, only 21% had a positive SLN (*18*). In a study of patients with breast cancer, 41% had a positive SLN (*19*). Realizing the need for non-invasive technology to identify SLNs, several lymphography technologies have been developed. However, while all of these techniques will identify the SLN, none can reliably identify LNs that harbor metastases.

Lymphoscintigraphy with ^{99m}Tc-sulfur colloids (^{99m}Tc-SCs), ^{99m}Tc-albumin colloids, or the recently approved ^{99m}Tc-Lymphoseek (*20*), as well as vital blue or fluorescent dyes (indocyanine green [ICG] or fluorescein) are all non-specific and can only be used to visualize an SLN without providing any information on the tumor status of the node. Percutaneous optical imaging of ICG detected even fewer LNs compared to lymphoscintigraphy (*21*). Of critical concern is the potential for displacement of macrophages in SLNs by tumor cells, which can lead to a negative scan. Negative mapping with lymphography using ^{99m}Tc-SC in patients with breast cancer has been associated with a higher number of tumor-positive SLNs not seen with lymphography but found on final pathology (*22*). The passage of these relatively large radiolabeled colloids can be blocked by tumor cells, thus limiting the clinical utility of this technique. Therefore, current methods do not accurately indicate the tumor status of the LN and, most alarmingly, may yield false-negative results.

Positron emission tomography (PET) imaging with intravenous (IV) ^{18}F-fluoro-2-deoxy-D-glucose (^{18}F-FDG) has not improved the detection of micrometastases (metastatic deposits <2 mm in size) in lymph nodes. ^{18}F-FDG PET imaging often fails to detect LN stations with metastases in normal-sized LNs in many cancers. In endometrial cancer, PET/computed tomography (CT) had a sensitivity of only 17% to detect metastases in normal-sized LNs (*23*), in melanoma only 14% (*24*), and in breast cancer only 48% (*19*). A recent study compared ^{18}F-FDG PET with diffusion-weighted imaging (DWI) in patients with uterine cancers and concluded

5

that neither DWI nor PET/CT were sufficiently accurate to replace lymphadenectomy. For small metastatic LNs, DWI and PET/CT showed a detection sensitivity of 75% and 16.7%, respectively (*25*). A meta-analysis showed that the overall accuracy of gadolinium-enhanced magnetic resonance imaging (MRI) for the detection of nodal metastases is only moderate as well (*26*).

Since micrometastasis in SLNs carries a significant negative prognostic value in many solid tumors, new imaging techniques to detect these relevant nodal metastases are urgently needed. To this end, we recently developed "positron lymphography" (PLG) (*27*). In PLG, ^{18}F-FDG is injected *locally* near or around the tumor and is then transported via the lymphatic channels to the draining SLN with high signal-to-noise ratio even in higher echelon nodes in preclinical studies (*27*)]. We already demonstrated the feasibility of ^{18}F-FDG/PET imaging of the lymphatic system using intradermal ^{18}F-FDG injection in a healthy murine cohort verifying both uptake in SLNs and the ability to use ^{18}F-FDG as a radiotracer (*27*). Our more recent work subsequently demonstrated the differential ^{18}F-FDG uptake in tumor-positive LNs versus normal SLNs in a melanoma murine model (*28*). Importantly, in dynamic studies, the uptake in tumor-positive LNs was significantly different from that in negative SLNs, allowing the identification of micrometastases (*29*). The small size of the tracer (e.g., glucose, 0.9 nm compared to SC, ~90 nm) allows passage through channels infiltrated with tumor cells, and the molecular function of the tracers allows their uptake by tumor cells, which is not achieved by any of the currently used colloid agents. And in contrast to PET with IV injection of the tracer, local injection in PLG assures a high signal in the draining LNs with little background signal anywhere else in the initial phase. This is particularly important in the pelvis, where high uptake in the bladder and bowel can obscure small LNs. PLG constitutes a new approach in lymphography, moving from current localization techniques to the characterization of SLNs based on molecular markers for cancer and lymphatic flow.

We hypothesized that PLG may provide more precise LN delineation with minimal background signal in the early phase of imaging and improve upon conventional PET/CT and SLN mapping techniques to identify SLNs and delineate malignant from benign nodes. Our first-in-human pilot study tests our hypothesis by expanding upon an extensive body of work on the SLN biopsy technique and rationale of using PLG as a primary modality. This involves a local, intracervical ^{18}F-FDG injection combined with PET/CT imaging. The primary goal of this pilot study was to evaluate the feasibility of intracervical injection of ^{18}F-FDG for PLG to (i) identify SLN(s) and (ii) identify tumor-positive SLN(s). The ability to do so would represent an invaluable new tool for surgeons performing SLN biopsy, providing them pre-operatively with a three-dimensional PET/CT map indicating the presence of tumor-positive nodes to be removed.

Materials and Methods

Patient Selection: This prospective pilot study targeted enrollment of 20 evaluable patients for CT-based pelvic PLG on the day of their scheduled surgery for stage IB1 cervical cancer or staging surgery for high-grade endometrial cancer. Patients with high-grade endometrial tumors were selected in order to enrich for a higher proportion of occult LN-positive cases. Our protocol received institutional review board approval prior to patient enrollment, and all patients signed an informed consent form prior to participation (https://clinicaltrials.gov/ct2/show/NCT02285192). This protocol was deemed in compliance with the Health Insurance Portability and Accountability Act.

Positron Lymphography: Intracervical ^{18}F-FDG applications are not routinely used in medical imaging; therefore, dosimetry curves were generated prior to the study and are provided in Appendix 1. Based on calculated organ absorbed and effective dose estimates, a total dose

range of 8-12 mCi (296-444 MBq) was administered to the cervix. The mean total dose injected

was 11.5 mCi (426.9 MBq). Enrolled patients underwent intracervical injection of ^{18}F-FDG in the

PET suite. With the patient already positioned on the scanner's table (GE Discovery STE), a

gynecologic oncologist inserted a speculum to visualize the intravaginal cervix and then [18]F-

FDG was administered via syringe both superficially and deep to the face of the cervix at the 3

and 9 o'clock positions. Immediately after injection, dynamic PET/CT imaging (i.e., the PLG) of

the pelvic region was obtained over 30 minutes (one bed position, approximately from the aortic

bifurcation to the symphysis) followed by a whole-body PET/CT acquisition performed as a 30-

minute (in the first few patients, 60 minutes) late-phase scan. IV contrast was administered only

for the pelvic CT to allow for better contrast in the pelvic PLG while the late-phase, whole-body

scan is acquired as a standard PET/CT with a reduced-dose, non-contrast CT. Since the PLG

was performed on the day of surgery, no oral contrast was applied.

Data collection included standard uptake value (SUV) and the anatomic location of pelvic and

para-aortic LNs from PLG; all excised SLNs were evaluated perioperatively with a hand-held

gamma probe. Intraoperative data, including the identification and anatomic location of pelvic

and para-aortic SLNs was also collected. Pre-operative and intra-operative findings were

correlated with postoperative pathologic findings in the SLNs.

Image Analysis: All analyses were performed immediately after imaging acquisition on a

standard clinical GE Centricity workstation equipped with an Advanced Workstation (AW)

analysis suite. The readers were board-certified nuclear medicine physicians (JG, NPT), and

one reader was both board certified in radiology and nuclear medicine (JG). Analysis of the

dynamic series is not possible with AW; therefore, 6 time points were extracted (every 5 minutes

up to 30 minutes) and evaluated. The maximum SUV (SUV max) was determined from nodes

that were visible on early time points on the dynamic PET and then followed over time to

visualize the course of uptake. At a later time point, a dedicated analysis of the dynamic study was performed using Hermes analysis software (Hermes Medical Solutions, Stockholm, Sweden). The nodal SUVs of the dynamic study were fit to a decreasing mono-exponential function to derive the time-activity curve of the individual LN. Any SLNs identified during the early analysis following PLG were recorded and communicated to the surgeons with the intention for removal during the standard staging surgery on the day of PLG. Removal of an SLN was confirmed by measuring ex vivo radioactivity in the LN with a handheld positron probe (Node Seeker; IntraMedical Imaging, Hawthorne, CA). On PLG, a suspicious LN was defined as any primary draining pelvic LN with a substantially sustained or increased SUV over time, relative to each patient's individual background. This was individualized to each patient and discussed with the surgeon for each case, as the SUVs in some patients reached values of several hundred, while in others it remained low, probably depending upon variations in the injection.

Additional image reconstructions, showing the bones, vessels, and PET data as maximum-intensity rendered PET/CT overlay, were performed with the GE PACS system, which was used to demonstrate the data to the surgical team. In addition, OsiriX (Open Source licensing – LGPL) was used for further visualization.

Surgery: Following PLG, each patient underwent a standard staging surgery that included SLN mapping. The Gynecology Service within the Department of Surgery at Memorial Sloan Kettering Cancer Center (MSK) uses an evidence-based standard algorithm for SLN mapping (Appendix 2). This algorithm includes intracervical injection of vital blue dye or ICG for intraoperative fluorescent detection of SLNs. The uterine lymphatics take up the ICG, and patients map in one of two dominant patterns, with rare exceptions (Appendix 3). The SLN is the first draining LN to take up colored dye. Any additional LNs that take up dye may be removed

but are not considered SLNs. By adhering to these standard algorithms, the results of the PLG did not influence clinical decision making; removal of additional LNs suspicious on PLG but not considered SLNs was left to the surgeon's discretion.

If the PET imaging protocol identified SLNs other than those identified intraoperatively with dye, these LNs were removed in addition to the nodes identified by the standard algorithm. LN basins were defined in relation to vascular landmarks. These additional LNs removed were labeled as experimental LNs and were included in the tabulation of nodes considered discordant between the PET/CT and dye protocol. All LNs removed and identified as SLNs were subjected to the Clinical Laboratory Improvement Amendment (CLIA)-certified pathologic ultrastaging protocol, which is the standard at our institution for SLN pathologic assessment. Appendix 4 details the pathologic ultrastaging protocol.

Analysis: Two detection methods were evaluated for accuracy in detecting SLNs—PLG and the clinical standard dye-assisted intraoperative SLN technique. Discordant SLNs were noted and descriptively reported. The primary endpoint at the nodal level was number of SLNs found using the dye technique and whether PLG was able to identify the same or additional SLNs. Successful mapping based on patient level data was described as follows: the success rate of PLG as a mapping technique was compared with the conventional dye technique as our institutional gold standard to identify SLNs. Patients who mapped at least unilaterally were counted as having had successful mapping. Descriptive statistics were used to clarify the percent unilateral versus percent bilateral LN mapping, and used to make rough comparisons (at the patient level) between PLG and dye-assisted intraoperative SLN mapping technique success rates.

In order to distinguish between tumor-positive and tumor-negative SLNs in women undergoing

surgical staging for stage IB1 cervical cancer and high-grade endometrial cancer, we assessed

SUV on dynamic phase imaging during PLG and generated time-activity curves using ^{18}F-FDG

update values over multiple time points. Based on our preclinical data (*28, 29*), suspicious

SLNs, i.e., tumor-containing LNs, were expected to show a different uptake pattern from normal

LNs, particularly a delayed peak or increasing uptake over time.

The SUV max and the time-to-peak measured in individual LNs from the PLG was compared

with the pathologic assessment (benign vs. malignant) of each labeled LN. An intraoperative

gamma probe was used for an objective evaluation of the radioactivity and, most importantly, to

confirm that the right node with uptake was resected. Therefore, all experimentally identified

SLNs were determined using objective measures.

Sensitivity at the level of nodal data was calculated for PLG. Exact specificity could not be

determined, since a full LN dissection for endometrial and cervical cancers is no longer a

standard surgical procedure at our institution, so the true negative LN rate cannot be reported.

As in all diagnostic testing, the goal is to maximize sensitivity without sacrificing specificity. In

this study, maximizing sensitivity remains important, but without a full LN dissection, we were

unable to calculate the false-positive rate. The proportion of patients with at least one false-

positive LN was reported.

Any possible adverse events associated with intracervical ^{18}F-FDG were also reported. We

collected and reported data on demographic characteristics, surgical procedures performed,

and intraoperative characteristics in a descriptive manner.

Results

Twenty-three patients gave consent to undergo PLG. Two withdrew consent prior to undergoing

PLG and one patient's PLG scan was not assessable due to significant beam-hardening artifacts from a left hip prosthesis, leaving 20 patients evaluable for this study. Median age was 61 years (range, 26-81 years). The median body mass index (BMI) was 26.2 kg/m^2 (range, 20-42 kg/m^2). During surgery, 4 patients (20%) were administered lymphazurin blue dye and 16 (80%) were administered ICG for intraoperative standard SLN mapping. Of the 20 patients undergoing PLG, 15 (75%) had endometrial and 5 (25%) had cervical cancer. All endometrial cancers were of high-grade histologic subtypes; the cervical tumors included 4 adenocarcinomas and 1 squamous cell carcinoma (Table 1). Of the 15 patients with endometrial cancer, 11 (73%) had stage I disease (uterus confined) on final pathology. Of the 5 patients with cervical cancer, 4 (80%) had stage I disease (cervix confined) on final pathology. A median of 5 LNs were removed (range, 0-15 LNs) across all patients evaluated.

The median dose of ^{18}F-FDG injected into the cervix was 11.6 mCi (range, 10.0-12.8 mCi). Four patients had failed PLG mapping, and 1 patient did not undergo SLN removal at the time of surgery. There were 8 patients (40%) with bilateral and 8 (40%) with unilateral PLG mapping, for a combined successful mapping rate of 80%. One patient did not undergo SLN mapping in the OR, and of the 19 who mapped using the SLN dye technique in the OR, all 19 (100%) mapped bilaterally. There were 3 (15%) node-positive cases on final pathologic analysis, 2 endometrial and 1 cervical cancer, and 100% of these cases were detected by PLG, among them, 1 with a focus of only 80 tumor cells within a single LN. There were 2 (10%) false-positive cases with PLG, suggesting positive SLNs and final pathology of the corresponding SLN negative for tumor. Table 1 summarizes demographic, disease, and imaging characteristics. There were no study-related adverse events noted in all 20 patients enrolled to the study protocol.

True Positive Cases

Three patients had true positive SLNs detected by both PLG and SLN mapping, and these were confirmed on final pathology. As already observed in our preclinical study (*28, 29*), ^{18}F-FDG uptake in tumor-positive LNs followed a pattern on the dynamic PLG different from that of benign LNs. Figure 1 demonstrates a patient with endometrial carcinosarcoma (stage IIIC1) who had unilateral PLG mapping on the right to 3 SLNs. Of the 3 LNs identified with PLG on the right, there was one right obturator SLN that demonstrated a delayed, prolonged ^{18}F-FDG uptake pattern with a late peak, as shown in the time-activity curve. This was different from the 2 additional SLNs seen on the right that demonstrated lower overall ^{18}F-FDG uptake with a benign uptake pattern, i.e., an early peak and then rapid decline. The right obturator SLN seen on PLG with a unique uptake pattern corresponded to a right obturator SLN identified in the OR and was confirmed with ex vivo radioactivity measurement. Final pathology of this LN revealed 80 tumor cells within the node (see Figure 1 inset pathology photo). The patient did not map with PLG on the left side; however, a left external iliac SLN was identified and removed in the OR and found to be benign on final pathologic evaluation.

Patients 5 and 15 also had true positive nodes as detected by both PLG and intraoperative SLN mapping, confirmed on final pathology. Patient 5 had serous endometrial cancer. Her PLG revealed a prolonged ^{18}F-FDG uptake that was only slowly decreasing over each time point (Figure 2). The PLG-positive SLN corresponded to a left obturator SLN in the OR, confirmed as radioactive with the hand-held device upon removal. Pathology revealed 2 micrometastatic foci measuring 2 mm and 3 mm in this node. A right external iliac/obturator PLG SLN was also identified using PLG; however, this node did not demonstrate any suspicious ^{18}F-FDG uptake and was interpreted as negative on PLG. This right-sided SLN was found to be positive, with an 11-mm tumor focus on final pathology. Patient 15 was diagnosed with a clinically stage IBI cervical adenocarcinoma. This patient demonstrated unilateral PLG mapping with prolonged

^{18}F-FDG uptake within a right external iliac/obturator SLN. This corresponded to a right obturator SLN. Final pathology revealed this excised specimen to contain 2 nodes, one that was positive for tumor cells (Figure 2).

Micromorphometry of Nodes

We examined the micromorphometric features of each of the positive SLNs found in the study cohort. Each of the 3 cases exhibited distinct micromorphometric features. Patient 1 had a single positive SLN with a microscopic focus of a total of approximately 80 tumor cells seen, consisting of multiple deposits of single cells and small clusters within a subcapsular sinus. Tumor deposits represented <1% of the total LN volume. Patient 5 had 2 positive SLNs identified, 1 identified with PLG. The left obturator SLN revealed 2 micrometastatic tumor foci on pathologic evaluation. Micromorphometric analysis revealed a single tumor deposit occupying 60% of the LN with an infiltrative, nodular pattern of tumor growth. The right obturator SLN was not seen with PLG, as there was no definite mapping to the side, and was described as an 11-mm tumor focus on pathologic evaluation. Micromorphometric evaluation revealed a single tumor deposit occupying 40% of the LN with the same infiltrative, nodular pattern of tumor growth as seen in the contralateral SLN. Patient 15 had a single positive SLN on the right that occupied 15% of the LN and was a single deposit of tumor with an expansile, nodular pattern of tumor growth. See Appendix 5 and 6 for complete micromorphometric descriptions and corresponding photographs.

Overall, all patients harboring positive nodes were identified. Based on the small number of positive lymph nodes in this cohort, it is difficult to draw any correlation between morphology, tumor density in the node, and PLG results. A large cohort of node-positive patients will be required to better correlate PLG results with morphometric characteristics of the positive nodes.

True Negative Cases

Of the 20 evaluable patients in the PLG cohort, there were 11 (55%) who underwent PLG who had a negative SLN both with PLG and SLN mapping in the OR as correlated with final pathologic evaluation. There were 4 patients who had failed mapping. Figure 3A, B highlights a negative case, in which bilateral PLG mapping was observed with nodes localizing to the external iliac nodal basins. On final pathology evaluation, these SLNs were found to be negative for tumor.

False Positive Cases

There were 2 patients (Patients 11 and 14) in the PLG cohort with positive SLNs seen on dynamic PET imaging. This was based on the pattern of ^{18}F-FDG uptake seen in the SLN. Most representative is a patient with high-grade endometrial cancer (Patient 11) showing unilateral PLG mapping with prolonged, increased, and a delayed peak of ^{18}F-FDG uptake within a right external iliac SLN suggestive of malignancy (Figure 3C, D). This corresponded to a right external iliac SLN identified at the time of surgery (concordant mapping). Final pathology showed the SLN was negative for tumor cells.

Discussion

In this cohort of 20 patients, we demonstrate the first-in-human experience of PLG in patients with endometrial or cervical cancers. Although this is primarily a study for feasibility in a human cohort, we also sought to learn more about uptake patterns in tumor-positive and tumor-negative SLNs on PLG and to correlate this information with intraoperatively identified SLNs and subsequent final pathology. We demonstrated the excellent sensitivity of this technique to identify tumor-positive LNs and also identified potential pitfalls that merit further evaluation and improvement. The number of reported false positive cases (10%) was relatively high, and this was in large part due to the pattern of uptake seen in the PLG-identified nodes during dynamic

phase imaging, which was either equivocal (but not clearly benign) or most consistent with the pattern of a positive LN. We have used our preclinical data to guide us on what constitutes normal versus suspicious uptake patterns in LNs. In our true positive SLN cases, there was a common pattern of delayed, prolonged ^{18}F-FDG uptake in SLNs on dynamic phase imaging that raised suspicion for malignancy. We also found that this feature was more subtle in some cases than in others. It is possible that with additional case experience, more than one positive uptake pattern may emerge.

A discussion and review of images immediately following PLG and before surgery allowed for the accurate localization and removal of the nodes seen on PLG. We encountered some challenges in identifying SLNs in certain locations, predominantly close to vessels and ureters due to a quick transition of the injected ^{18}F-FDG into the circulation. This transition occurred much faster than in our preclinical set up, probably largely due to different injection sites (intracervical in humans versus intracutaneous in mice). However, this is a commonly known limitation of ^{18}F-FDG use, as it is excreted quickly via the renal system. The use of IV contrast for the CT portion of PLG in the later cohort of patients partially helped to overcome this limitation. Given that the vast majority of SLNs in cervical and endometrial cancer will be found in the obturator space, which is immediately adjacent to the ureter, alternative tracers that are more specific to tumor and not excreted in the urine should be explored. This is the subject of ongoing work in our group. It is also conceivable that PLG using a PET/MR scanner could enhance soft tissue delineation, including genitourinary anatomy, and help overcome some of the challenges of a renally excreted radiotracer. Interestingly, the high activity at the cervical injection site was not a major limitation, mostly because most of the SLNs are found at the pelvic sidewall and not in the immediate vicinity of the cervix. However, there are potentially less complex anatomical sites in which PLG could be useful, e.g., in determining SLNs in breast cancer or melanoma.

We had initially allowed for 3 or fewer failed mapping cases in the first 10 patients evaluated before terminating our study for futility. We had 4 failed mappings in this study, with 2 in the first and 2 in the second set of 10 patients evaluated. Our initial estimate of successful mapping (at least unilateral) was set at 60% rather than 80% as with dye-based cervical injections, taking into account the experimental nature of this technique. A success rate of 80% mapping using PLG was noted, which was higher than anticipated and comparable to rates in the literature of SLN mapping using colored dye. Importantly, all surgeons performing injections for this study were experienced with the technique of cervical injections for SLN mapping. All but 1 patient in our cohort of 20 patients had successful bilateral mapping with ICG or vital blue dye. The 4 patients with failed mapping may be unique to the use of ^{18}F-FDG. More data are needed to better understand this finding.

Conclusion

PLG in patients with apparent early-stage cervical or endometrial cancer demonstrated 100% sensitivity in localizing positive SLNs. We report mapping success using ^{18}F-FDG in 80% of our cohort, which was higher than anticipated. All patients with tumor-positive SLNs were correctly identified; however, some of the individual positive SLNs in those patients were missed. The limitations of PLG include the rapid transition of the ^{18}F-FDG into the circulation and subsequent rapid renal excretion, which can limit the localization of pelvic SLNs and lead to a high number (10%) of false positive SLNs. Given the high sensitivity of this technique, further study is warranted, including the use of new tracers and improved imaging modalities to better visualize soft tissue structures adjacent to nodes.

Disclosure Statement

Key Points

QUESTION: Is there a way to characterize, rather than just locate, sentinel lymph nodes in tumor patients to guide the surgeons?

PERTINENT FINDINGS: In our pilot clinical trial 20 patients with cervical or high-grade endometrial cancer were evaluated with the novel approach of positron lymphography. All node-positive cases were correctly identified, including micrometastatic lymph nodes, demonstrating feasibility and its ability to identify patients with nodal metastases.

IMPLICATIONS FOR PATIENT CARE: Positron lymphography could be a valuable tool to detect tumor-positive lymph nodes prior to surgery and thus guide the surgeons and limiting complications from unnecessary lymphadenectomies.

References

1.   Gould EA, Winship T, Philbin PH, Kerr HH. Observations on a "sentinel node" in cancer of the parotid. *Cancer.* Jan-Feb 1960;13:77-78.

2.   Cabanas RM. An approach for the treatment of penile carcinoma. *Cancer.* Feb 1977;39(2):456-466.

3.   Abu-Rustum NR. The increasing credibility of sentinel lymph node mapping in endometrial cancer. *Annals of surgical oncology.* Feb 2013;20(2):353-354.

4.   Abu-Rustum NR, Khoury-Collado F, Pandit-Taskar N, et al. Sentinel lymph node mapping for grade 1 endometrial cancer: is it the answer to the surgical staging dilemma? *Gynecologic oncology.* May 2009;113(2):163-169.

5.   Cibula D, Abu-Rustum NR, Dusek L, et al. Bilateral ultrastaging of sentinel lymph node in cervical cancer: Lowering the false-negative rate and improving the detection of micrometastasis. *Gynecologic oncology.* Dec 2012;127(3):462-466.

6.   Khoury-Collado F, Murray MP, Hensley ML, et al. Sentinel lymph node mapping for endometrial cancer improves the detection of metastatic disease to regional lymph nodes. *Gynecologic oncology.* Aug 2011;122(2):251-254.

7.   Levenback CF, Ali S, Coleman RL, et al. Lymphatic mapping and sentinel lymph node biopsy in women with squamous cell carcinoma of the vulva: a gynecologic oncology group study. *Journal of clinical oncology : official journal of the American Society of Clinical Oncology.* Nov 1 2012;30(31):3786-3791.

8.   Rossi EC, Kowalski LD, Scalici J, et al. A comparison of sentinel lymph node biopsy to lymphadenectomy for endometrial cancer staging (FIRES trial): a multicentre, prospective, cohort study. *The Lancet Oncology.* Mar 2017;18(3):384-392.

9.   Network NCC. NCCN Clinical Practice Guidelines in Oncology: Uterine Neoplasms Version 2.2019. https://www.nccn.org/professionals/physician_gls/pdf/uterine.pdf. Accessed January 7, 2019.

10.   Abu-Rustum NR, Alektiar K, Iasonos A, et al. The incidence of symptomatic lower-extremity lymphedema following treatment of uterine corpus malignancies: a 12-year experience at Memorial Sloan-Kettering Cancer Center. *Gynecologic oncology.* Nov 2006;103(2):714-718.

11.   Achouri A, Huchon C, Bats AS, Bensaid C, Nos C, Lecuru F. Complications of lymphadenectomy for gynecologic cancer. *European journal of surgical oncology : the journal of the European Society of Surgical Oncology and the British Association of Surgical Oncology.* Jan 2013;39(1):81-86.

12.   Mariani A, Webb MJ, Keeney GL, Haddock MG, Calori G, Podratz KC. Low-risk corpus cancer: is lymphadenectomy or radiotherapy necessary? *American journal of obstetrics and gynecology.* Jun 2000;182(6):1506-1519.

13.   Barlin JN, Khoury-Collado F, Kim CH, et al. The importance of applying a sentinel lymph node mapping algorithm in endometrial cancer staging: beyond removal of blue nodes. *Gynecologic oncology.* Jun 2012;125(3):531-535.

14.   Burke TW, Levenback C, Tornos C, Morris M, Wharton JT, Gershenson DM. Intraabdominal lymphatic mapping to direct selective pelvic and paraaortic lymphadenectomy in women with high-risk endometrial cancer: results of a pilot study. *Gynecologic oncology.* Aug 1996;62(2):169-173.

15.   Cormier B, Diaz JP, Shih K, et al. Establishing a sentinel lymph node mapping algorithm for the treatment of early cervical cancer. *Gynecologic oncology.* Aug 2011;122(2):275-280.

16.   Levenback CF, van der Zee AG, Rob L, et al. Sentinel lymph node biopsy in patients with gynecologic cancers Expert panel statement from the International Sentinel Node Society Meeting, February 21, 2008. *Gynecologic oncology.* Aug 2009;114(2):151-156.

17.   Veronesi U, Paganelli G, Galimberti V, et al. Sentinel-node biopsy to avoid axillary dissection in breast cancer with clinically negative lymph-nodes. *Lancet (London, England).* Jun 28 1997;349(9069):1864-1867.

18.   Morton DL, Thompson JF, Cochran AJ, et al. Final trial report of sentinel-node biopsy versus nodal observation in melanoma. *The New England journal of medicine.* Feb 13 2014;370(7):599-609.

19.   Song BI, Kim HW, Won KS. Predictive Value of (18)F-FDG PET/CT for Axillary Lymph Node Metastasis in Invasive Ductal Breast Cancer. *Annals of surgical oncology.* Aug 2017;24(8):2174-2181.

20.   Baker JL, Pu M, Tokin CA, et al. Comparison of [(99m)Tc]tilmanocept and filtered

[(99m)Tc]sulfur colloid for identification of SLNs in breast cancer patients. *Annals of surgical*

oncology. Jan 2015;22(1):40-45.

21.   Namikawa K, Tsutsumida A, Tanaka R, Kato J, Yamazaki N. Limitation of indocyanine

green fluorescence in identifying sentinel lymph node prior to skin incision in cutaneous

melanoma. *International journal of clinical oncology.* Feb 2014;19(1):198-203.

22.   Brenot-Rossi I, Houvenaeghel G, Jacquemier J, et al. Nonvisualization of axillary

sentinel node during lymphoscintigraphy: is there a pathologic significance in breast cancer?

Journal of nuclear medicine : official publication, Society of Nuclear Medicine. Aug

2003;44(8):1232-1237.

23.   Kitajima K, Murakami K, Yamasaki E, et al. Accuracy of 18F-FDG PET/CT in detecting

pelvic and paraaortic lymph node metastasis in patients with endometrial cancer. *AJR American*

journal of roentgenology. Jun 2008;190(6):1652-1658.

24.   Singh B, Ezziddin S, Palmedo H, et al. Preoperative 18F-FDG-PET/CT imaging and

sentinel node biopsy in the detection of regional lymph node metastases in malignant

melanoma. *Melanoma research.* Oct 2008;18(5):346-352.

25.   Kitajima K, Yamasaki E, Kaji Y, Murakami K, Sugimura K. Comparison of DWI and

PET/CT in evaluation of lymph node metastasis in uterine cancer. *World journal of radiology.*

May 28 2012;4(5):207-214.

26.   Klerkx WM, Heintz AP, Mali WP, et al. Lymph node detection by MRI before and after a systematic pelvic lymphadenectomy. *Gynecologic oncology.* Aug 2009;114(2):315-318.

27.   Thorek DL, Abou DS, Beattie BJ, et al. Positron lymphography: multimodal, high-resolution, dynamic mapping and resection of lymph nodes after intradermal injection of 18F-FDG. *Journal of nuclear medicine : official publication, Society of Nuclear Medicine.* Sep 2012;53(9):1438-1445.

28.   Lockau H, Neuschmelting V, Ogirala A, Vilaseca A, Grimm J. Dynamic (18)F-FDG PET Lymphography for In Vivo Identification of Lymph Node Metastases in Murine Melanoma. *Journal of nuclear medicine : official publication, Society of Nuclear Medicine.* Feb 2018;59(2):210-215.

29.   Morton DL, Thompson JF, Essner R, et al. Validation of the accuracy of intraoperative lymphatic mapping and sentinel lymphadenectomy for early-stage melanoma: a multicenter trial. Multicenter Selective Lymphadenectomy Trial Group. *Annals of surgery.* Oct 1999;230(4):453-463; discussion 463-455.

Figure 1
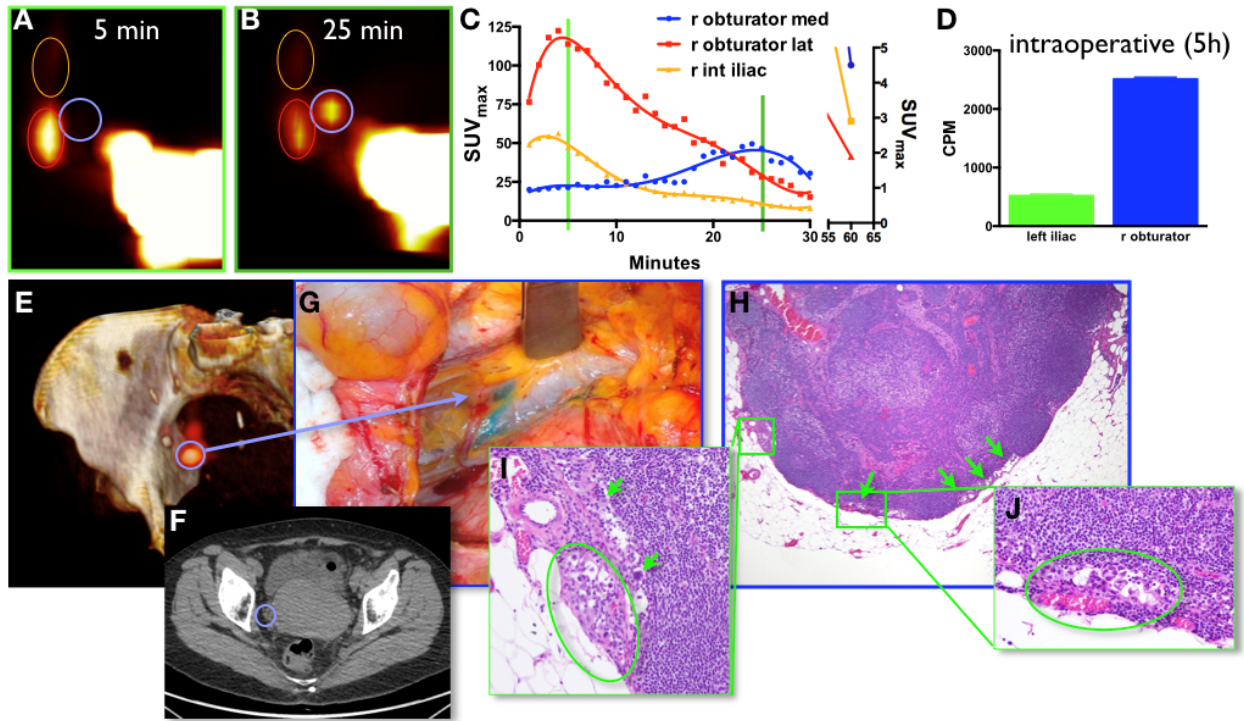
Figure 1: Representative example of clinical positron lymphography (PLG) with positron emission tomography/computed tomography (PET/CT) and intracervical injection of ^{18}F-fluoro-2-deoxy-D-glucose (^{18}F-FDG) in a patient with uterine carcinosarcoma (patient #1). (A, B) PLG demonstrated 3 sentinel lymph nodes (SLNs) in the right pelvis, **(B)** one of which demonstrated a prolonged and delayed uptake pattern, as shown in the time-activity curves **(C)**. **(D)** Intraoperative measurements of counts per minute (CPM) of the excised lymph nodes demonstrated even 5 h after tracer injection higher uptake in the suspicious node. **(E)** 3D surface reconstruction of the PET/CT at 25 minutes showing the higher uptake in the suspicious node (blue circle) and the same node shown on the axial CT **(F)**. **(G)** Intraoperative view of the node stained by vital blue dye. Histology - low **(H)** and high magnification **(I, J)** confirming the presence of metastatic carcinoma within the suspicious node.

Figure 2
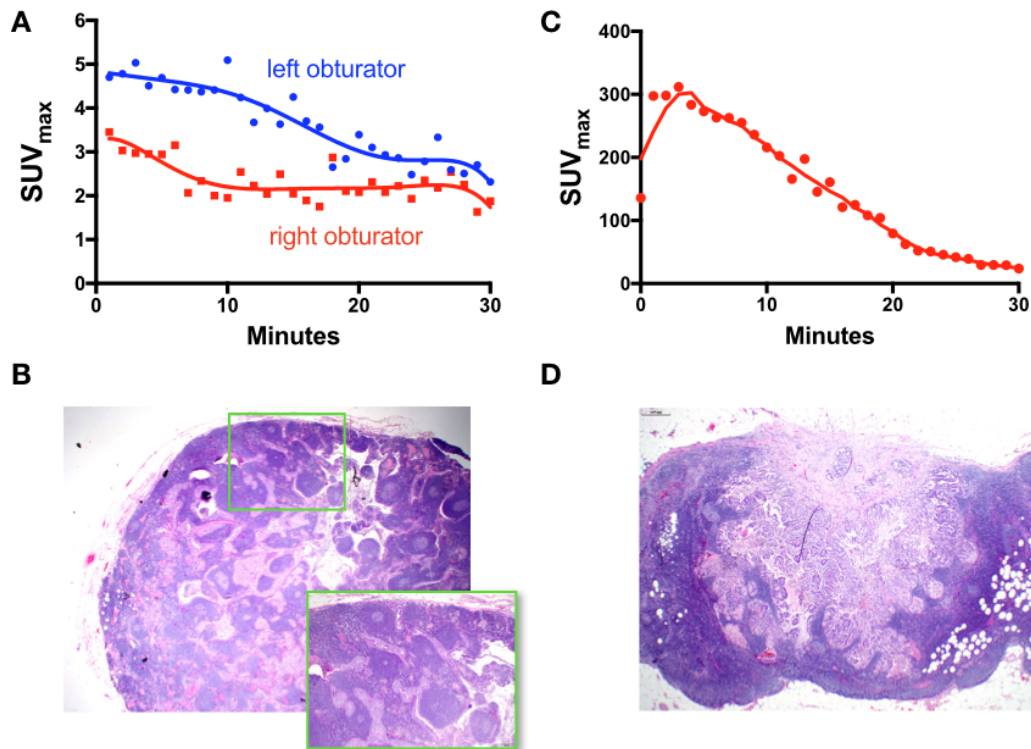
Figure 2: Positron lymphography (PLG) of tumor-positive lymph nodes. (A, B) Patient with serous endometrial cancer (Patient #5) in whom **A)** time-activity curve of a left obturator sentinel lymph node (SLN) demonstrated prolonged ^{18}F-fluoro-2-deoxy-D-glucose (^{18}F-FDG) uptake shoulder. This corresponded to a left obturator SLN, which was removed in the OR and revealed 2 micrometastatic tumor foci measuring 2 mm and 3 mm, respectively, on final pathology **(B)**. A right obturator PLG SLN was also identified, which did not demonstrate a prolonged uptake on time-activity curve (albeit not a rapid decrease either) and was interpreted as negative on PLG. This was identified and removed in the OR as a right SLN. On final pathology, this node was found to be positive, with an 11 mm metastatic tumor focus (not shown). **(C, D)** Patient with a stage IBI cervical adenocarcinoma (Patient #15) showing unilateral PLG mapping with delayed wash out of ^{18}F-FDG from a right external iliac/obturator SLN **(C)**. This resected specimen contained 2 lymph nodes, one that was positive for tumor cells, on final pathology **(D)**.

Figure 3
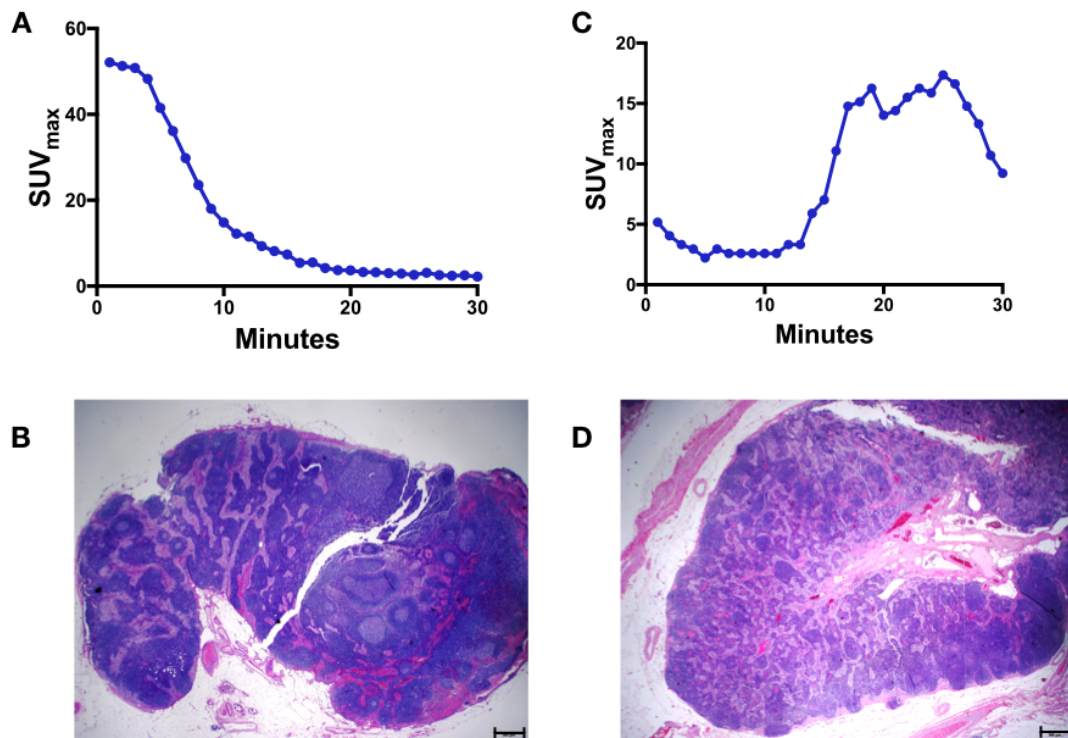
Figure 3: True negative and false positive positron lymphography (PLG). Patient with a high-grade endometroid adenocarcinoma and a left obturator sentinel lymph node (SLN) that was negative on **(A)** PLG and **(B)** pathology. **(C)** Patient with a high-grade endometrial cancer (Patient #11) showing unilateral PLG mapping with prolonged increase and a delayed peak of ^{18}F-fluoro-2-deoxy-D-glucose (^{18}F-FDG) uptake **(C)** within a right external iliac SLN, which was suggestive of malignancy**.** This corresponded to a right external iliac SLN at the time of surgery (concordant mapping), but final pathology revealed this SLN was negative for tumor cells **(D)**.

Table 1. Characteristics of patients undergoing positron lymphography (PLG) after intracervical ^{18}F-fluoro-2-deoxy-D-glucose (^{18}F-FDG) injection

ID	Age	BMI	Histology	Disease Site	Dye Used	PLG Mapping	Right	Left	OR Mapping	Right	Left	LN Removed	Path Positive SLN	PLG Positive SLN
1	67	25	Carcinosarcoma	Uterine	Vital Blue	Unilateral	Obturator		Bilateral	Obturator	External Iliac	15	Right Obturator	Obturator
2	81	41	Endometrioid	Uterine	ICG	Bilateral	External Iliac	External Iliac	Bilateral	External Iliac	External Iliac	3		
5	71	42	Serous	Uterine	ICG	Bilateral	External Iliac/Obturator	External Iliac/Obturator	Bilateral	Obturator	External iliac, Obturator	6	Left Obturator, Right Obturator	Left Obturator
6	67	26	Adenocarcinoma	Cervix	ICG	Bilateral	External Iliac	External Iliac	Bilateral	External Iliac	External Iliac	5		
7	57	31	Serous	Uterine	ICG	No Mapping			Bilateral	External Iliac	External iliac, Internal Iliac	4		
8	76	20	Carcinosarcoma	Uterine	ICG	Unilateral	External Iliac		Bilateral	External Iliac	External Iliac	2		
9	51	21	Dedifferentiated High grade	Uterine	ICG	No Mapping			Bilateral	External Iliac, Paraaortic	External iliac, Obturator	5		
10	67	32	adenocarcinoma High grade	Uterine	ICG	Bilateral	External Iliac	External Iliac	Bilateral	External Iliac	Obturator	5		
11	47	31	adenocarcinoma	Uterine	ICG	Unilateral	External Iliac		Bilateral	Obturator External iliac,	Internal Iliac External iliac,	4	No	Right External Iliac
13	43	35	Adenocarcinioma	Cervix	ICG	Bilateral	External Iliac	External Iliac	Bilateral	Internal Iliac	External Iliac External iliac,	5		Right External Iliac
14	40	23	Adenocarcinoma	Cervix	Vital Blue	Bilateral	External Iliac	External Iliac	Bilateral	Internal Iliac	Obturator	11	No	Iliac

No	Age	BMI	Histology	Site	Dye									
15	61	24	Adenocarcinoma	Cervix	Vital Blue	Unilateral	External Iliac, Obturator		Bilateral	External iliac, Obturator	External iliac, Internal Iliac	6	Right Obturator	Right External Iliac/Obturator
16	70	20	Carcinosarcoma	Uterine	ICG	Unilateral		Internal Iliac	Bilateral	External Iliac	External Iliac	3		
17	60	28	Serous	Uterine	ICG	Unilateral		External Iliac	Bilateral	External Iliac	External Iliac	5		
18	68	28	Serous	Uterine	ICG	No Mapping			Bilateral	Obturator	Obturator	5		
19	66	22	Endometrioid	Uterine	ICG	No Mapping			Bilateral	Internal Iliac	External iliac, Obturator	6		
20	26	21	Squamous Cell Carcinoma	Cervix	ICG	Bilateral	Internal Iliac	Internal Iliac, Parametria	Bilateral	Internal Iliac, Obturator	Internal Iliac, Obturator	4		
21	61	26	Serous	Uterine	Vital Blue	Unilateral		External Iliac	No mapping			0		
22	58	30	Endometrioid	Uterine	ICG	Bilateral	Common Iliac	External Iliac	Bilateral	Iliac bifurcation, Obturator	Obturator	7		
23	54	27	Endometrioid	Uterine	ICG	Unilateral		Obturator	Bilateral	External Iliac	External Iliac, Obturator	12		

BMI, body mass index; PLG, positron lymphography; LN, lymph node; SLN, sentinel lymph node; ICG, indocyanine green

Supplemental Figure 1

Study: Positron Lymphography High Grade Endometrial Cancer

Surgery Form
Patient Name_____ Date_____
MRN_____ Study ID_____
SLN Modality _____

Right   **Aorta**   **Left**

Left side tables:

HIGH PARA-AORTICS	A1	A2	A3	A4	A5
Dye+ Yes/No					
Predict Malignent/Benign					
Sentinel Yes/No					
Path Label (ex:"Left ingunial LN")					
positron lymphography (list ID)					

LOW PARA-AORTICS	A1	A2	A3	A4	A5
Dye+ Yes/No					
Predict Malignent/Benign					
Sentinel Yes/No					
Path Label (ex:"Left ingunial LN")					
positron lymphography (list ID)					

Common Iliac	A1	A2	A3	A4	A5
Dye+ Yes/No					
Predict Malignent/Benign					
Sentinel Yes/No					
Path Label (ex:"Left ingunial LN")					
positron lymphography (list ID)					

External Iliac	A1	A2	A3	A4	A5
Dye+ Yes/No					
Predict Malignent/Benign					
Sentinel Yes/No					
Path Label (ex:"Left ingunial LN")					
positron lymphography (list ID)					

Obturator	A1	A2	A3	A4	A5
Dye+ Yes/No					
Predict Malignent/Benign					
Sentinel Yes/No					
Path Label (ex:"Left ingunial LN")					
positron lymphography (list ID)					

Center bottom table (Internal Iliac):

A1	A2	A3	A4	A5	Internal Iliac	A1	A2	A3	A4	A5
					Dye+ Yes/No					
					Predict Malignent/Benign					
					Sentinel Y/N					
					Path Label (ex. "left ingunal LN"					
					positron lymphography (list ID)					

Right side tables:

HIGH PARA-AORTICS	A1	A2	A3	A4	A5
Dye+ Yes/No					
Predict Malignent/Benign					
Sentinel Yes/No					
Path Label (ex:"Left ingunial LN")					
positron lymphography (list ID)					

LOW PARA-AORTICS	A1	A2	A3	A4	A5
Dye+ Yes/No					
Predict Malignent/Benign					
Sentinel Yes/No					
Path Label (ex:"Left ingunial LN")					
positron lymphography (list ID)					

Common Iliac	A1	A2	A3	A4	A5
Dye+ Yes/No					
Predict Malignent/Benign					
Sentinel Yes/No					
Path Label (ex:"Left ingunial LN")					
positron lymphography (list ID)					

External Iliac	A1	A2	A3	A4	A5
Dye+ Yes/No					
Predict Malignent/Benign					
Sentinel Yes/No					
Path Label (ex:"Left ingunial LN")					
positron lymphography (list ID)					

Obturator	A1	A2	A3	A4	A5
Dye+ Yes/No					
Predict Malignent/Benign					
Sentinel Yes/No					
Path Label (ex:"Left ingunial LN")					
positron lymphography (list ID)					

Supplemental Figure 1: Anatomic reference chart used by surgeon and study radiologist to facilitate positron lymphography (PLG) sentinel lymph node (SLN) location and concordance with dye-identified SLN.

Supplemental Table 1.
Comparing investigational SLN mapping (A) and blue and green dye SLN mapping (B) with final pathology at the nodal level (n=113).

A. Investigational SLN mapping

Investigational SLN mapping negative Pathology negative	71	Investigational SLN mapping negative Pathology positive	NA
Investigational SLN mapping positive Pathology negative	15	Investigational SLN mapping positive Pathology positive	27
Total number of nodes	86		27

B. Dye SLN mapping

				Total
Dye SLN mapping negative Pathology negative	86	Dye SLN mapping negative Pathology positive	27	113
Dye SLN mapping positive Pathology negative	NA	Dye SLN mapping positive Pathology positive	NA	NA

NA = full LN dissection was not performed and number of nodes is unknown

Supplemental Table 2.
Comparing investigational SLN mapping (A) and blue and green dye SLN mapping (B) with final pathology at the patient level (n=20).

A. Investigational SLN mapping

Investigational SLN mapping negative Pathology negative	15	Investigational SLN mapping negative Pathology positive	0
Investigational SLN mapping positive Pathology negative	2	Investigational SLN mapping positive Pathology positive	3
Total number of patients	17		3

B. Dye SLN mapping

					Totals
Dye SLN mapping negative Pathology negative	17	Dye SLN mapping negative Pathology positive	3	20	
Dye SLN mapping positive Pathology negative	NA	Dye SLN mapping positive Pathology positive	NA	NA	

NA = full LN dissection was not performed and number of nodes is unknown

Supplemental Table 3.
Comparing investigational SLN mapping with blue and green dye SLN mapping at the (A) nodal and (N) patient level.

A. Node level (n=113)

| Dye SLN mapping negative Investigational SLN mapping negative	71	Dye SLN mapping positive Investigational SLN mapping negative	NA
Dye SLN mapping negative Investigational SLN mapping positive	42	Dye SLN mapping positive Investigational SLN mapping positive	NA

A. Patient level (n=20)

Dye SLN mapping negative Investigational SLN mapping negative	15	Dye SLN mapping positive Investigational SLN mapping negative	NA
Dye SLN mapping negative Investigational SLN mapping positive	5	Dye SLN mapping positive Investigational SLN mapping positive	NA

NA = full LN dissection was not performed and number of nodes is unknown

Organ	Diagnostic CAP-CT (per impaCT) (MSKCC Female mean) mGy/scan	Systemic (per ICRP-106, 2008) mGy/MBq	Cervical LN (per OLINDA) mGy/MBq	8 mCi Administration Systemic Frac 50% 4 mCi mGy	8 mCi Administration Cervical LN Frac 50% 4 mCi mGy	8 mCi Administration Total PET/CT Organ Dose Estimate mGy	10 mCi Administration Systemic Frac 50% 5 mCi mGy	10 mCi Administration Cervical LN Frac 50% 5 mCi mGy	10 mCi Administration Total PET/CT Organ Dose Estimate mGy	12 mCi Administration Systemic Frac 50% 6 mCi mGy	12 mCi Administration Cervical LN Frac 50% 6 mCi mGy	12 mCi Administration Total PET/CT Organ Dose Estimate mGy
Adrenals	1.35E+01	1.20E-02	2.70E-03	1.8E+00	4.0E-01	1.6E+01	2.2E+00	5.0E-01	1.6E+01	2.7E+00	6.0E-01	1.7E+01
Bladder	1.42E+01	1.30E-01	9.62E-02	1.9E+01	1.4E+01	4.8E+01	2.4E+01	1.8E+01	5.6E+01	2.9E+01	2.1E+01	6.4E+01
Bone surfases	2.03E+01	1.10E-02	5.19E-03	1.6E+00	7.7E-01	2.3E+01	2.0E+00	9.6E-01	2.3E+01	2.4E+00	1.2E+00	2.4E+01
Brain	1.61E+01	3.80E-02	1.48E-05	5.6E+00	2.2E-03	2.2E+01	7.0E+00	2.7E-03	2.3E+01	8.4E+00	3.3E-03	2.5E+01
Breasts	1.20E+01	8.80E-02	5.91E-04	1.3E+01	8.7E-02	2.5E+01	1.6E+01	1.1E-01	2.8E+01	2.0E+01	1.3E-01	3.2E+01
Gallbladder	1.44E+01	1.30E-02	1.04E-02	1.9E+00	1.5E+00	1.8E+01	2.4E+00	1.9E+00	1.9E+01	2.9E+00	2.3E+00	2.0E+01
Gastrointestinal tract												
- stomach	1.44E+01	1.10E-02	4.96E-03	1.6E+00	7.3E-01	1.7E+01	2.0E+00	9.2E-01	1.7E+01	2.4E+00	1.1E+00	1.8E+01
- small intestine	1.35E+01	1.20E-02	6.32E-02	1.8E+00	9.4E+00	2.5E+01	2.2E+00	1.2E+01	2.7E+01	2.7E+00	1.4E+01	3.0E+01
- colon		1.30E-02		1.9E+00		1.9E+00	2.4E+00		2.4E+00	2.9E+00		2.9E+00
- Upper large intestine	1.35E+01	1.20E-02	3.26E-02	1.8E+00	4.8E+00	2.0E+01	2.2E+00	6.0E+00	2.2E+01	2.7E+00	7.2E+00	2.3E+01
- Lower large intestine	1.27E+01	1.40E-02	3.54E-02	2.1E+00	5.2E+00	2.0E+01	2.6E+00	6.5E+00	2.2E+01	3.1E+00	7.9E+00	2.4E+01
Heart	1.53E+01	6.70E-02	1.14E-03	9.9E+00	1.7E-01	2.5E+01	1.2E+01	2.1E-01	2.8E+01	1.5E+01	2.5E-01	3.0E+01
Kidneys	1.47E+01	1.70E-02	5.66E-03	2.5E+00	8.4E-01	1.8E+01	3.1E+00	1.0E+00	1.9E+01	3.8E+00	1.3E+00	2.0E+01
Liver	1.38E+01	2.10E-02	4.05E-03	3.1E+00	6.0E-01	1.8E+01	3.9E+00	7.5E-01	1.8E+01	4.7E+00	9.0E-01	1.9E+01
Lungs	1.53E+01	2.00E-02	8.00E-04	3.0E+00	1.2E-01	1.8E+01	3.7E+00	1.5E-01	1.9E+01	4.4E+00	1.8E-01	2.0E+01
Muscles	9.59E+00	1.00E-02	1.16E-02	1.5E+00	1.7E+00	1.3E+01	1.9E+00	2.1E+00	1.4E+01	2.2E+00	2.6E+00	1.4E+01
Oesophagus		1.20E-02		1.8E+00		1.8E+00	2.2E+00		2.2E+00	2.7E+00		2.7E+00
Ovaries	1.26E+01	1.40E-02	1.27E-01	2.1E+00	1.9E+01	3.3E+01	2.6E+00	2.3E+01	3.9E+01	3.1E+00	2.8E+01	4.4E+01
Pancreas	1.32E+01	1.30E-02	4.30E-03	1.9E+00	6.4E-01	1.6E+01	2.4E+00	8.0E-01	1.6E+01	2.9E+00	9.5E-01	1.7E+01
Red marrow	1.12E+01	1.10E-02	1.22E-02	1.6E+00	1.8E+00	1.5E+01	2.0E+00	2.3E+00	1.5E+01	2.4E+00	2.7E+00	1.6E+01
Skin	8.56E+00	7.80E-03	3.28E-03	1.2E+00	4.9E-01	1.0E+01	1.4E+00	6.1E-01	1.1E+01	1.7E+00	7.3E-01	1.1E+01
Spleen	1.34E+01	1.10E-02	3.62E-03	1.6E+00	5.4E-01	1.6E+01	2.0E+00	6.7E-01	1.6E+01	2.4E+00	8.0E-01	1.7E+01
Thymus	1.69E+01	1.20E-02	4.77E-04	1.8E+00	7.1E-02	1.9E+01	2.2E+00	8.8E-02	1.9E+01	2.7E+00	1.1E-01	2.0E+01
Thyroid	2.16E+01	1.00E-02	1.25E-04	1.5E+00	1.9E-02	2.3E+01	1.9E+00	2.3E-02	2.3E+01	2.2E+00	2.8E-02	2.4E+01
Uterus	1.38E+01	1.80E-02	5.64E+00	2.7E+00	8.3E+02	8.5E+02	3.3E+00	1.0E+03	1.1E+03	4.0E+00	1.3E+03	1.3E+03
Remaining organs		1.20E-02		1.8E+00		1.8E+00	2.2E+00		2.2E+00	2.7E+00		2.7E+00
Effective Dose	1.34E+01 mSv/scan	1.90E-02 mSv/MBq	1.78E-01 mSv/MBq	2.8E+00 mSv	2.6E+01 mSv	4.3E+01 mSv/8 mCi	3.5E+00 mSv	3.3E+01 mSv	5.0E+01 mSv/10 mCi	4.2E+00 mSv	4.0E+01 mSv	5.7E+01 mSv/12 mCi

Appendix 2. Gynecologic Oncology Sentinel Lymph Node Mapping Algorithm
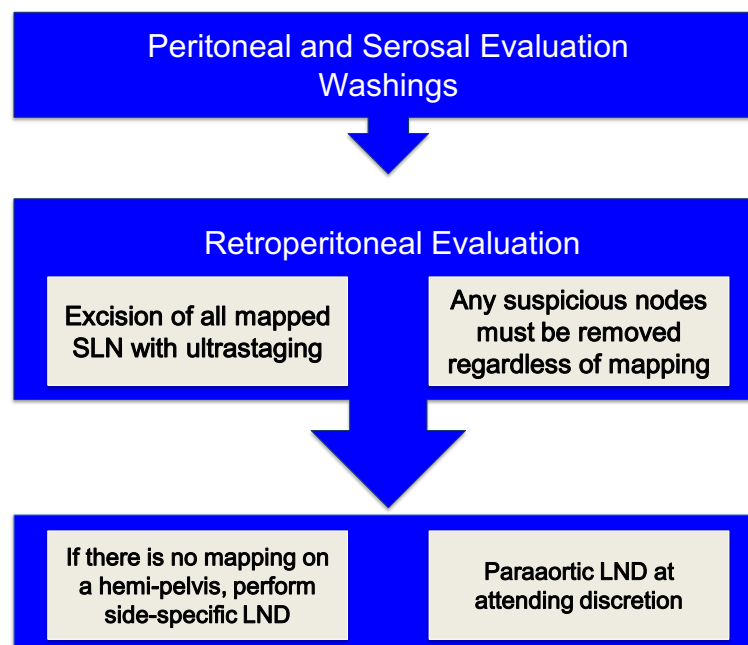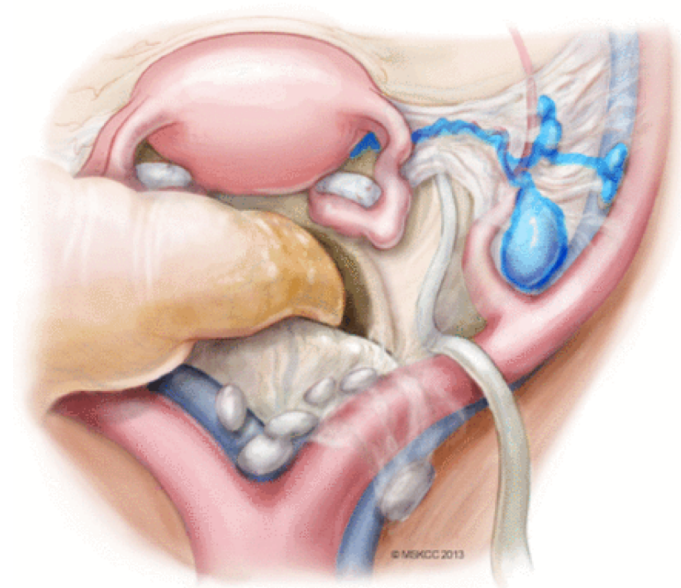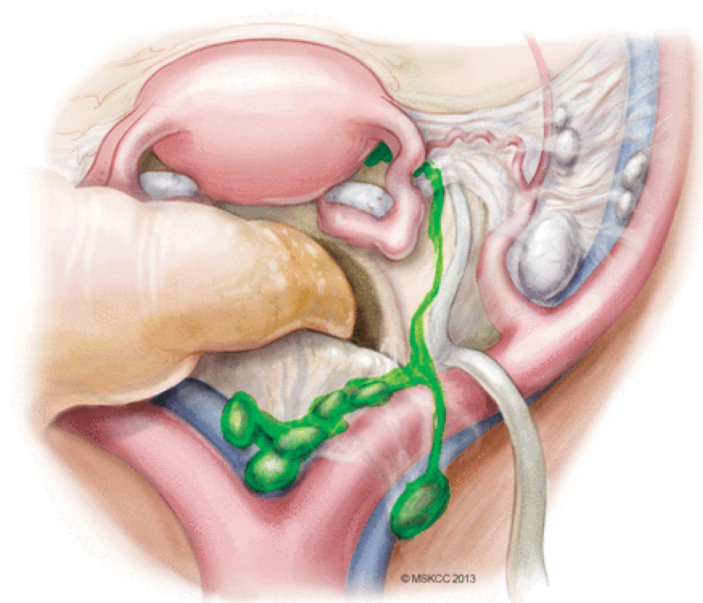

SLN, sentinel lymph node; LND, lymph node dissection

Barlin JN, Khoury-Collado F, Kim CH, et al. The importance of applying a sentinel lymph node mapping algorithm in endometrial cancer staging: beyond removal of blue nodes. Gynecol Oncol 2012; 125: 531–5.

# Appendix 3. Dominant patterns for sentinel lymph node mapping after intracervical injection.

A.

B.

A. The most common sentinel lymph node location after a cervical injection are medial to the external iliac vessels, ventral to the hypogastric vessels, and in the superior portion of the obturator space. B. The less common sentinel lymph node locations of sentinel lymph nodes are seen when channels travel within the mesoureter cephalad to the common iliac vessels and presacral region.

Appendix 4. Ultrastaging technique for sentinel lymph nodes in endometrial and cervical cancer.
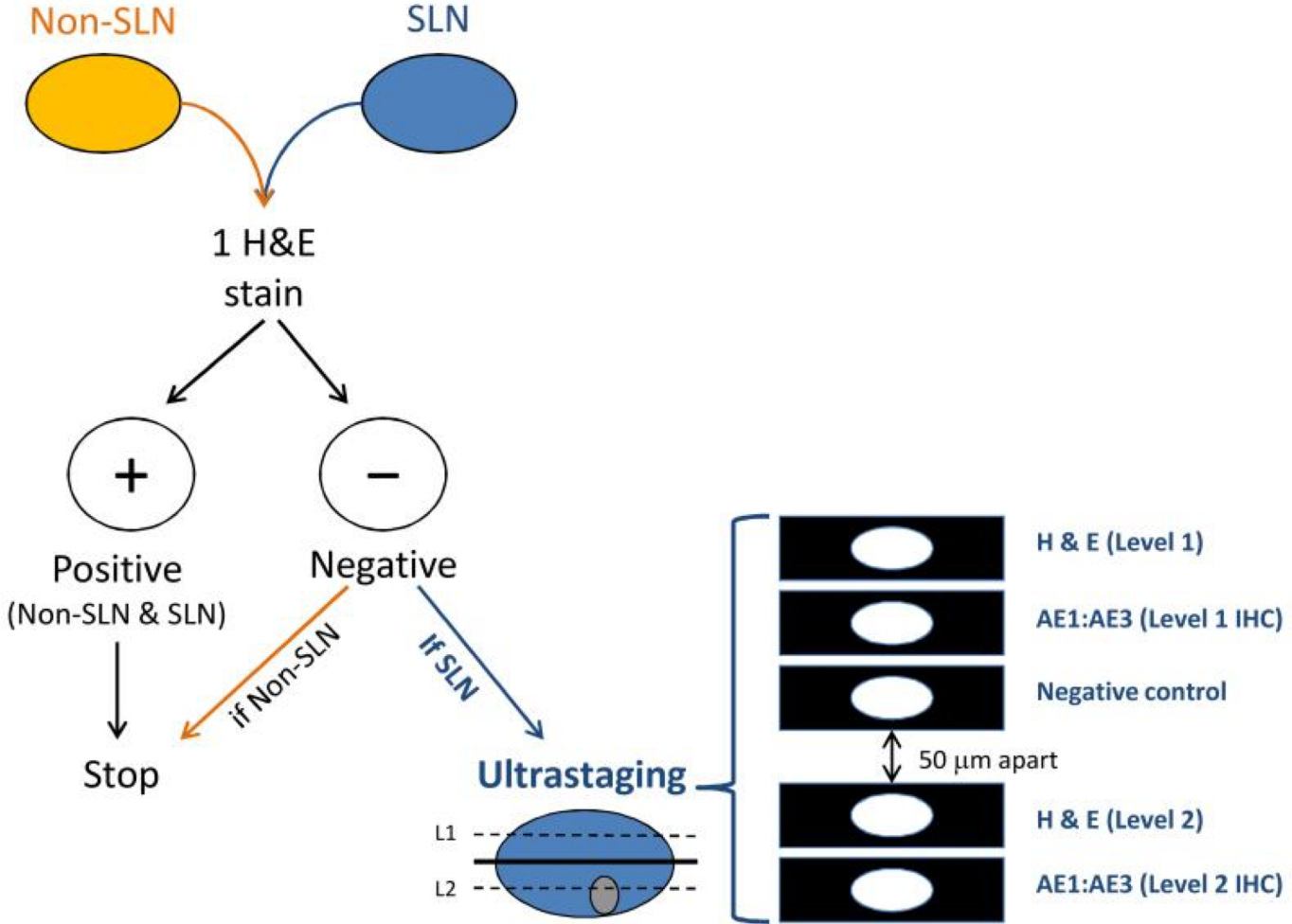
Kim CH, Soslow RA, Park KJ, Barber EL, Khoury-Collado F, Barlin JN, Sonoda Y, Hensley ML, Barakat RR, Abu-Rustum NR. Pathologic Ultrastaging Improves Micrometastasis Detection in Sentinel Lymph Nodes during Endometrial Cancer Staging. Int J Gynecol Cancer. 2013 Jun;23(5): 964-970.

Appendix 5. Micromorphometry of positive nodes.

Micromorphometric features of SLN deposits

Histology	ID	SLN No.	No. of deposits	Size (mm)	% of LN	Subcapsular depth (mm)	Shape/ Distribution
Endometrial Carcinosarcoma	1	R obt 1/1 +	Multiple	See 'Shape'	<1	0	Single cells and small clusters (<0.1mm) within subcapsular sinus, spanning a maximum length of 3.0mm
Endocervical AC	5	R Obt 1/2 +	1	4.2x3.0	15	3.0	Nodule, expansile
Endometrial serous	15	L Obt 1/5 +	1	10.0x6.0	60	6.0	Nodule, infiltrative
		R Obt 1/1+	1	8.0x8.0	40	8.0	Nodule, infiltrative

Appendix 5. Micromorphometry of positive nodes.
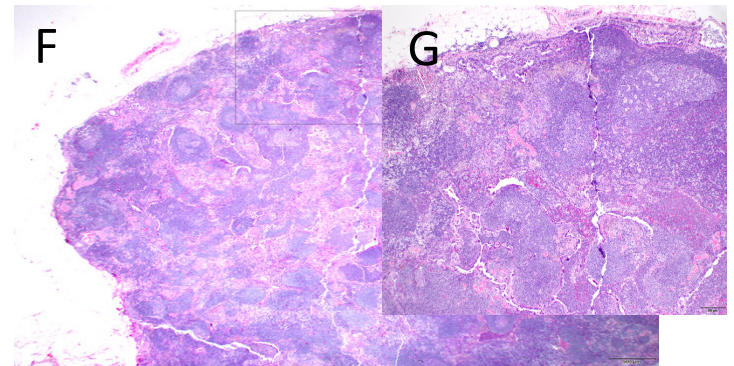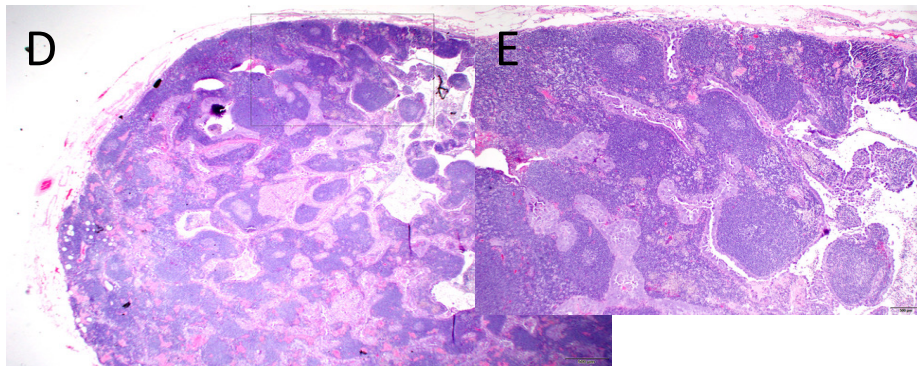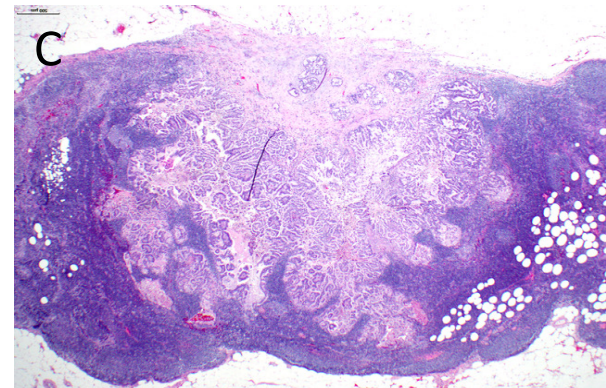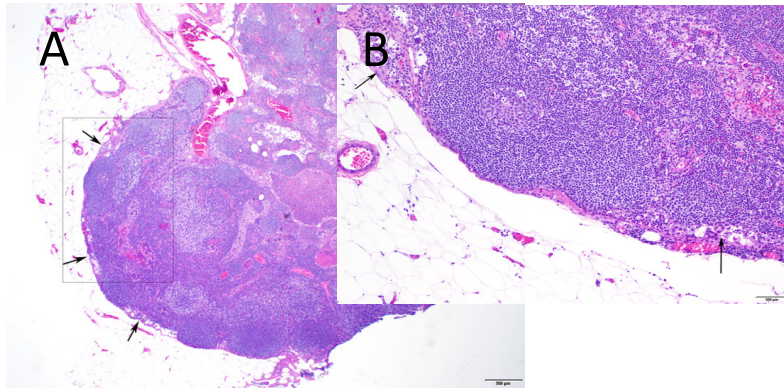
(A.) Patient ID 1. Deposits (arrows) of metastatic carcinomatous component of carcinosarcoma in subcapsular sinus of lymph node, low-power view of lymph node; (B) area denoted by rectangle in (A).

(C.) Patient ID 5. Single expansile nodular deposit of metastatic adenocarcinoma extending from capsule of lymph node into the nodal parenchyma.

(D.) Patient ID 15. Nodular deposit of metastatic serous carcinoma extending from capsule of lymph node into the parenchyma. The tumor nodule comprises cords and glands infiltrating between nodal parenchyma, low-power; (E.) area denoted by rectangle in (D).

(F.) Patient ID 15. Nodular deposit of metastatic serous carcinoma extending from capsule of lymph node into the parenchyma. The tumor nodule comprises cords and glands infiltrating between nodal parenchyma, low-power; (G.) area denoted by rectangle in (F).

See Appendix 4 for complete micromorphometric descriptions.